Titan's thermospheric response to various plasma environments

J. H. Westlake,[1] J. M. Bell,[2] J. H. Waite Jr.,[1,2] R. E. Johnson,[3] J. G. Luhmann,[4] K. E. Mandt,[2,5] B. A. Magee,[2] and A. M. Rymer[6]

Received 28 October 2010; revised 8 December 2010; accepted 11 January 2011; published 23 March 2011.

[1] The Cassini-Huygens mission has been observing Titan since October 2004, resulting in over 70 targeted flybys. Titan's thermosphere is sampled by the Ion and Neutral Mass Spectrometer (INMS) during several of these flybys. The measured upper atmospheric density varies significantly from pass to pass. In order to quantify the processes controlling this variability, we calculate the nitrogen scale height for a variety of parameters related to the solar and plasma environments and, from these, we infer an effective upper atmospheric temperature. In particular, we investigate how these calculated scale heights and temperatures correlate with the plasma environment. Measured densities and inferred temperatures are found to be reduced when INMS samples Titan within Saturn's magnetospheric lobe regions, while they are enhanced when INMS samples Titan in Saturn's plasma sheet. Finally the data analysis is supplemented with Navier-Stokes model calculations using the Titan Global Ionosphere Thermosphere Model. Our analysis indicates that, during the solar minimum conditions prevailing during the Cassini tour, the plasma interaction plays a significant role in determining the thermal structure of the upper atmosphere and, in certain cases, may override the expected solar-driven diurnal variation in temperatures in the upper atmosphere.

Citation: Westlake, J. H., J. M. Bell, J. H. Waite Jr., R. E. Johnson, J. G. Luhmann, K. E. Mandt, B. A. Magee, and A. M. Rymer (2011), Titan's thermospheric response to various plasma environments, *J. Geophys. Res.*, *116*, A03318, doi:10.1029/2010JA016251.

1. Introduction

[2] Saturn's largest moon Titan has a dense, extended atmosphere consisting primarily of nitrogen and methane. When Titan is immersed within Saturn's magnetospheric plasma, it experiences characteristic electron temperatures and densities of approximately 100–1000 eV and 0.1–1 cm^{-3}, respectively [*Coates*, 2010]. This plasma is composed primarily of oxygen ions, protons, and electrons. Titan is a solid, conducting obstacle with no significant internal magnetic field to deflect the oncoming plasma flow, giving the plasma direct access to the upper thermosphere/exobase region. The plasma environment near Titan has been observed to be highly variable, depending on the moon's location within Saturn's magnetosphere [*Rymer et al.*, 2009]. Occasional excursions out of Saturn's magnetosphere expose Titan to shocked solar wind plasma [*Bertucci et al.*, 2008]. Saturn's magnetospheric configuration is described as a magnetodisk containing a warped plasma sheet, which moves in and out of Titan's orbit depending on several factors including: (1) solar wind parameters, (2) an asymmetry in Saturn's magnetosphere causing a thicker and generally more dense plasma sheet on the dayside, and (3) the periodic perturbations or flapping of the current sheet [*Arridge et al.*, 2008; *Bertucci et al.*, 2008]. Given this dynamic plasma environment, the Titan plasma interaction is currently suspected to play a significant and highly variable role in the upper atmospheric energetics, dynamics, and composition [*De La Haye et al.*, 2007a; *Bell et al.*, 2010a; *Johnson*, 2009; *Johnson et al.*, 2009].

[3] The thermosphere of Titan is the uppermost region of Titan's collision-dominated atmosphere, lying below the quasi-collisionless exosphere. On most planetary bodies, the thermosphere is characterized by a positive thermal gradient with altitude; however, Titan's thermal structure is poorly constrained [cf. *Bell et al.*, 2010a] and, because of this, thermosphere configurations that exhibit positive, negative, and flat temperature gradients have been proposed [cf. *Bell et al.*, 2010b; *Yelle et al.*, 2006; *Müller-Wodarg et al.*, 2008; *Strobel*, 2008, 2009].

[4] Measurements of the atmospheric density made by the Cassini Ion and Neutral Mass Spectrometer (INMS) suggest a nearly isothermal region extending from ~1100 km up to

[1]Department of Physics and Astronomy, University of Texas at San Antonio, San Antonio, Texas, USA.
[2]Space Science and Engineering Division, Southwest Research Institute, San Antonio, Texas, USA.
[3]Engineering Physics Program, University of Virginia, Charlottesville, Virginia, USA.
[4]Space Sciences Laboratory, University of California, Berkeley, California, USA.
[5]Department of Environmental and Civil Engineering, University of Texas at San Antonio, San Antonio, Texas, USA.
[6]Johns Hopkins University Applied Physics Laboratory, Laurel, Maryland, USA.

0148-0227/11/2010JA016251

the exobase at ~1500 km [*Waite et al.*, 2005]. Temperatures inferred from individual flyby data range from 116 K to 200 K and exhibit large deviations between similarly oriented flybys [*Waite et al.*, 2005, 2007]. Temperatures obtained from the Cassini Ultraviolet Imaging Spectrograph (UVIS) instrument yielded a temperature between 148 K and 151 K in the thermosphere [*Shemansky et al.*, 2005]. Reanalysis of the Voyager Ultraviolet Spectrometer (UVS) data yielded effective temperatures of 152.9 K and 157.7 K for the dusk and dawn flanks, respectively [*Vervack et al.*, 2004]. The Huygens probe measured thermospheric temperatures ranging between 140 K and 160 K with large wave-like perturbations [*Fulchignoni et al.*, 2005]. Studies of Titan's thermospheric thermal structure in the northern hemisphere have also proposed zonal, meridional, and diurnal dependencies [*Müller-Wodarg et al.*, 2008; *Cui et al.*, 2009].

1.1. Overview of Titan's Plasma Environment

[5] Plasma from Saturn's magnetosphere deposits energy through collisional processes that occur between the energetic ions and electrons and the neutral atmosphere of Titan. This interaction is very complex and varies significantly with spatial location around Titan [see, e.g., *Sittler et al.*, 2009; *Coates*, 2010]. Magnetospheric electron distributions are observed to be highly variable in density and temperature as classified by *Rymer et al.* [2009] using the Cassini Plasma Spectrometer's Electron Spectrometer (CAPS-ELS) data. This investigation, covering the flybys TA-T55, identified four broad interaction types: plasma sheet, magnetosheath, bimodal, and lobe-like electron distributions. The plasma sheet and bimodal distributions generally contained the highest-electron energies and densities. The magnetosheath interactions occur when Titan is out of Saturn's magnetosphere and exposed to shocked solar wind plasma, exhibiting high-density low-temperature electron distributions. The lobe electron distributions are similar in energy to the plasma sheet distributions but are generally an order of magnitude lower in density; these occur when Titan is above or below the plasma sheet but still within Saturn's magnetosphere.

[6] A magnetic field investigation of the near-Titan plasma environment extending from TA-T62 has been performed, concentrating on the ±8 h around the Titan encounter [*Simon et al.*, 2010]. Portions of the flybys are characterized as being within either lobe or plasma sheet type fields with distinctions made for northern and southern lobe regions. Encounters occurring during Saturn Local Times (SLTs) of 0900 UT to 1500 UT, or within the noon sector magnetosphere, were found to be embedded in a broad, highly perturbed current sheet regime, while those occurring within the midnight sector magnetosphere (SLT of 2100 UT to 0300 UT) were found to be in a significantly thinner, more transient current sheet prone to large vertical fluctuations. Thus, the electron distribution analysis by *Rymer et al.* [2009] and the magnetic field analysis by *Simon et al.* [2010] shows consistency in their identification of the plasma environment during the targeted Titan flybys relevant to the INMS.

[7] Plasma sheet electrons are characterized by peak electron energies of 120 to 600 eV and fluxes at the peak energy of 3.5×10^5 to 1.2×10^6 cm^{-2} s^{-1} sr^{-1}. In contrast, the lobe plasma consists of similar peak electron energies (150 to 820 eV) but are generally an order of magnitude lower in flux (5.3×10^4 to 2.4×10^5 cm^{-2} s^{-1} sr^{-1}). A systematic study of the ion populations within the various plasma regimes has indicated that the classification schemes in the electron data correspond to the ions as well [*Nemeth et al.*, 2009]. The heavy ion populations, which are likely dominated by O^+ ions, in the plasma sheet are similar in energy to those in the lobe flybys but are in general an order of magnitude greater in flux [*Nemeth et al.*, 2009]. Bimodal flybys appear to contain a significant amount of heavy ions while the magnetosheath flybys appear to consist primarily of lighter ions such as H^+. The O^+ ions have been suggested previously by *Shah et al.* [2009] to be the dominant source of energy for the upper atmosphere.

[8] The regions in which plasma has access to the atmosphere are dependent on the flow direction, electric fields, and magnetic fields. Titan is tidally locked to Saturn meaning that the same side of Titan faces Saturn at all times during its orbit. Therefore, longitude on Titan corresponds directly to the region of the plasma interaction as shown in Figure 1. The flow overtakes Titan causing the heavy ions such as oxygen to deposit their energy primarily on the side in which the faster corotating plasma impacts Titan which is referred to as the ram side or trailing hemisphere with some spreading to the Saturn-facing flank [*Sillanpää et al.*, 2007]. The convection electric field is expected to point radially away from Saturn when the magnetic field is roughly dipolar in shape. In this configuration, the convection electric field forces the pickup ions into the atmosphere on the Saturn-facing side and away from the atmosphere on the anti-Saturn-facing side [*Hartle et al.*, 2006; *Michael and Johnson*, 2005; *Tseng et al.*, 2008]. Also, as discussed by *Coates* [2010] and *Sittler et al.* [2009], the wake region of Titan is most likely experiencing electron precipitation along the near radially draped field lines in that region.

1.2. Solar EUV/UV Influence

[9] Solar EUV/UV photons are absorbed in the thermosphere, resulting in heating from excitation, dissociation, and ionization of the neutral atmosphere. Solar influence varies with several well-known parameters: (1) the time of day on Titan, (2) the solar zenith angle, (3) obliquity of Titan and the instantaneous distance between Titan and the Sun (i.e., seasonal effects), and (4) the solar activity. Calculations by *De La Haye et al.* [2008] showed that solar processes were dominant over electron precipitation below 1150 km. This study did not consider magnetospheric ions which have been shown to penetrate much further into the thermosphere [*Cravens et al.*, 2008]. The resulting modeled temperature profiles varied from 127.9 K to 156.3 K with the majority of the deviation due to day/night asymmetries. The majority of the Cassini INMS mission to date has occurred during solar minimum conditions, meaning that the solar influence over Titan's upper atmosphere has been at its relative weakest during the observations.

1.3. The Purpose of This Study

[10] This study compiles the INMS atmospheric mass density measurements from the TA-T61 flybys to assess the impact of the plasma environment on the thermal structure of the upper atmosphere. Within this study we compare to previous work to evaluate assertions made regarding the parameters controlling the thermal structure, however we focus on the effect of the plasma environment. Specifically we assess

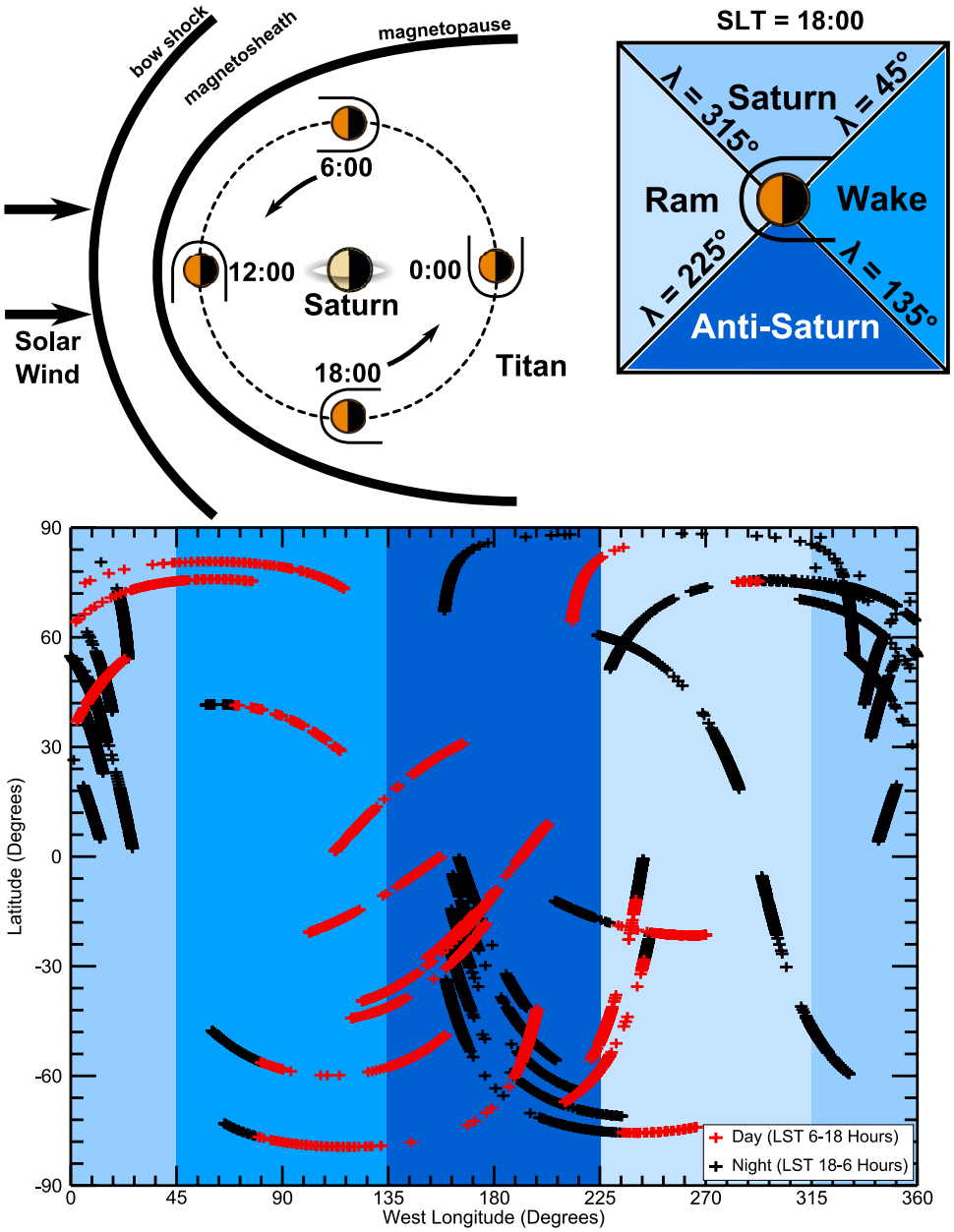

Figure 1. The spatial coverage of the flybys investigated in this work is shown. (top left) Shown diagrammatically are the possible solar and plasma orientations. (top right) The regions of Titan's local plasma interaction as they are oriented with respect to west longitude (λ). (bottom) The latitude versus the west longitude of the INMS data considered in this study; the regions are colored to correspond to the plasma interaction sectors called out in the top right image. The red crosses correspond to the dayside, while the black crosses correspond to the nightside.

how the upper atmospheric thermal structure responds to the presence or absence of the plasma sheet. The Titan Global Ionosphere Thermosphere Model (T-GITM) of *Bell et al.* [2010a] is used to further interpret the results. Furthermore, this study aims to assay the relative importance of the solar and plasma influences on Titan's upper atmosphere.

2. Instrumentation and Methodology

[11] From October 2004 to January 2010 the INMS sampled Titan's atmosphere during many targeted flybys. Table 1 summarizes the data analyzed in this study which are taken from the closed source of the Cassini INMS for 29 flybys. The method used for reducing the INMS data to obtain the N_2 and CH_4 densities is detailed by *Magee et al.* [2009]. The geospatial details and conditions during the flybys considered in this study are detailed in Table 1 with trajectories shown in Figure 1. The INMS densities are corrected by a factor of 3 to account for a cross calibration factor between the INMS, NAV, and AACS [*Bell et al.*, 2010a].

[12] The N_2 densities are analyzed using the following procedure. Assuming that the atmosphere is hydrostatic and

Table 1. The Details of the Flybys Considered in This Study[a]

			Closest Approach						
Flyby	Date	SLT (h)	Alt (km)	ϕ (°)	λ (°)	SZA (°)	LST (h)	F10.7	Plasma Classification
TA	26 Oct 2004	10.6	1174	38.8	88.4	91.1	16.8	137	PS
T5	16 Apr 2005	5.3	1025	74.0	272.0	127.5	23.3	77	PS
T16	22 Jul 2006	2.4	950	85.1	316.3	105.4	17.4	74	
T18	23 Sep 2006	2.3	962	70.9	357.0	89.8	14.4	71	Lobe
T19	09 Oct 2006	2.2	980	60.9	357.5	81.0	14.3	75	PS
T21	12 Dec 2006	2.1	1000	43.1	264.7	125.2	20.3	102	
T23	13 Jan 2007	2.0	1000	30.6	357.9	53.3	14.0	79	PS
T25	22 Feb 2007	13.9	1000	30.4	17.3	161.2	0.57	76	
T26	10 Mar 2007	13.8	981	31.7	357.9	149.5	1.76	70	BM
T28	10 Apr 2007	13.7	991	50.4	358.1	137.2	1.67	69	
T29	26 Apr 2007	13.7	981	59.4	358.4	129.8	1.60	81	PS
T30	12 May 2007	13.6	960	68.6	358.9	121.7	1.53	71	
T32	13 Jun 2007	13.6	975	84.5	1.5	106.9	0.3	71	MS
T36	02 Oct 2007	11.5	973	−59.9	108.9	67.3	16.1	66	PS
T39	20 Dec 2007	11.4	970	−70.2	176.6	61.2	11.5	73	PS
T40	05 Jan 2008	11.3	1010	−11.7	130.4	37.6	14.5	80	BM
T41	22 Feb 2008	11.2	1000	−34.9	151.8	30.2	13.0	72	Lobe
T42	25 Mar 2008	11.1	1000	−27.2	156.4	21.3	12.6	89	MS
T43	12 May 2008	11.0	1000	20.7	142.0	35.9	13.8	68	Lobe
T48	05 Dec 2008	10.4	960	−10.4	178.7	25.0	10.4	69	
T49	21 Dec 2008	10.3	970	−44.1	236.8	82.6	6.5	68	PS
T50	07 Feb 2009	10.2	960	−33.8	306.5	136.7	1.8	71	
T51	27 Mar 2009	10.1	960	−30.6	234.8	84.1	6.4	67	PS
T55	21 May 2009	22.0	965	−21.9	177.9	141.4	21.9	72	PS
T56	06 Jun 2009	21.9	965	−32.0	178.1	135.0	21.8	69	Lobe*
T57	22 Jun 2009	21.9	955	−42.0	178.4	127.8	21.8	68	PS*
T58	08 Jul 2009	21.8	965	−52.1	178.8	120.2	21.7	71	PS*
T59	24 Jul 2009	21.8	955	−62.2	179.6	112.2	21.6	68	PS*
T61	25 Aug 2009	21.7	970	−19.2	237.1	85.9	17.7	67	Lobe*

[a]The altitude, latitude, west longitude, and solar zenith angle is given at the closest approach to Titan. The F10.7 cm solar flux refers to that observed at 1 AU and is given in solar flux units (sfu) which are equivalent to 10^{-22} W m^{-2} Hz^{-1}. The plasma classifications are the following: plasma sheet (PS), bimodal (BM), lobe, and magnetosheath (MS). The starred plasma identifications are preliminary CAPS-ELS observations and are consistent with *Simon et al.* [2010].

in diffusive equilibrium the number density of a major neutral species is then determined by

$$n_s(z) = n_s(z_0)\frac{T_s(z_0)}{T_s(z)}\exp\left(-\int_{z_0}^{z}\frac{dz'}{H_s}\right) \quad (1)$$

where $n_s(z)$ is the number density of species s, z_0 is the reference altitude, T_s is the species temperature, and H_s is the scale height of species s. Assuming that the scale height is invariant with the altitude, linear fits to the logarithm of the N_2 density are performed. To restrict the fits to be within the thermosphere the altitude of the exobase is estimated by equating the mean free path with the scale height. The mean free path for species s within a gas mixture containing several other gases i is estimated as

$$\lambda_s = \frac{1}{n_s\sigma_{ss}\sqrt{2} + \sum_{i\neq s} n_i\sigma_{is}\sqrt{1 + m_s/m_i}}. \quad (2)$$

[13] Where σ_{ij} is the collision cross section of species i interacting with species j which is estimated using the hard sphere radii of the molecules in the following expression

$$\sigma_{ij} = \pi\left(r_i + r_j\right)^2 \quad (3)$$

where r_i and r_j are the hard sphere radii of the gases i and j, respectively [*Chapman and Cowling*, 1952]. The exobase is calculated considering the atmosphere to consist of N_2, and CH_4, whose hard sphere radii were taken to be 2.07×10^{-8}cm and 2.34×10^{-8}cm. N_2 is the dominant species in the thermosphere, therefore we calculate its exobase and use it to set the upper boundary of the fit.

[14] This method produces a scale height which is averaged over a few hundred kilometers in altitude. Within this region the gravitational acceleration is decreasing with altitude. To account for the decline in g the altitude is replaced with a surface referenced geopotential altitude defined as

$$z - z_0 = \frac{h - h_0}{1 + (h - h_0)/r_0}, \quad (4)$$

where r_0 is the reference height, in this case the radius of Titan and h represents the physical altitude above the reference [*Banks and Kockarts*, 1973]. Placing the reference h_0 at the surface then accounts for the nonnegligible (~20%) decrease in gravitational acceleration over the altitude range. This geopotential altitude, z, then directly replaces the physical altitude and is used in the fits.

[15] The effective temperature, T_{eff} is then derived from the scale height as

$$H_s = \frac{kT_{eff}}{m_s g_0}, \quad (5)$$

where k is Boltzmann's constant, m_s is the mass of species s, and g_0 is the gravitational acceleration at the reference

Table 2. Presented are the Effective Temperatures and Exobase Heights for the Listed Groupings[a]

	T_{Eff} (K)	Exobase Height (km)
Global average	153.0 ± 1.2	1537
Plasma sheet	160.7 ± 1.0	1542
Lobe	131.7 ± 1.2	1407
Bimodal	145.1 ± 1.9	1517
Magnetosheath	144.3 ± 1.8	1547

[a]The fits are taken over the altitude range 1050 km to the calculated exobase height.

surface, in this case the surface of Titan. N_2 is relatively inert and due to its dominance in the upper atmosphere its effective temperature can in general be regarded as a good indicator of the effective temperature of the atmosphere as a whole.

[16] The scale height determination is solely dependent on the change in density, therefore the absolute calibration of the INMS is irrelevant and only the precision of the measurement becomes important. This model is based upon the simple assumptions of a hydrostatic, isothermal, and N_2 dominated atmosphere and is in general not susceptible to uncertainties due to systematic density perturbations occurring outside of the altitude range studied. For example if a heating process occurred a few scale heights below the boundary of the model it is plausible that the increased density and upwelling would become a factor in the upper atmosphere. This effect is studied in Appendix A in which simulated Cassini flybys are produced considering a simplistic model atmosphere. The results from Appendix A show that the effective temperature deviations caused by geospatial density perturbations are of the order of a few degrees Kelvin. Furthermore, this study does not assume that horizontal density deviations are greater than temporal deviations.

3. Results

[17] Table 2 and Figure 2 give the results of the scale height fits over the entirety of the INMS data. When considering the complete data set the effective temperature is found to be 153.0 ± 1.2 K. This corresponds to a scale height of about 74 km in physical altitude and 35 km in geopotential altitude. The dayside and nightside sampling appears to be roughly uniform, producing a mean solar zenith angle of the measurements is 97.0 which is roughly consistent with a diurnal mean of 90.0. The average F10.7 cm solar radio flux for this investigation was 76 s.f.u indicating that the solar flux was well within solar minimum conditions throughout the study. The longitude coverage of the orbit synchronous satellite is mostly on the Saturn and anti-Saturn facing sectors with 30% and 38% of the coverage, respectively, and the corotational ram and wake sectors containing 17% and 15%, respectively.

3.1. Global Plasma Influence

[18] Based on only a few data sets, *De La Haye et al.* [2007a] suggested that there was evidence for a plasma effect. Here we show using an extensive data set and Cassini data on the plasma that a magnetospheric effect is likely as can be seen in Figure 3 and Table 2. The high-density high-energy plasma sheet flybys show an effective temperature of 160.7 ± 1.0 K while the low-plasma density, low-energy lobe flybys show an effective temperature of 131.7 ± 1.2 K. The 29.0 K effective temperature increase observed between the plasma sheet encounters versus the lobe encounters is

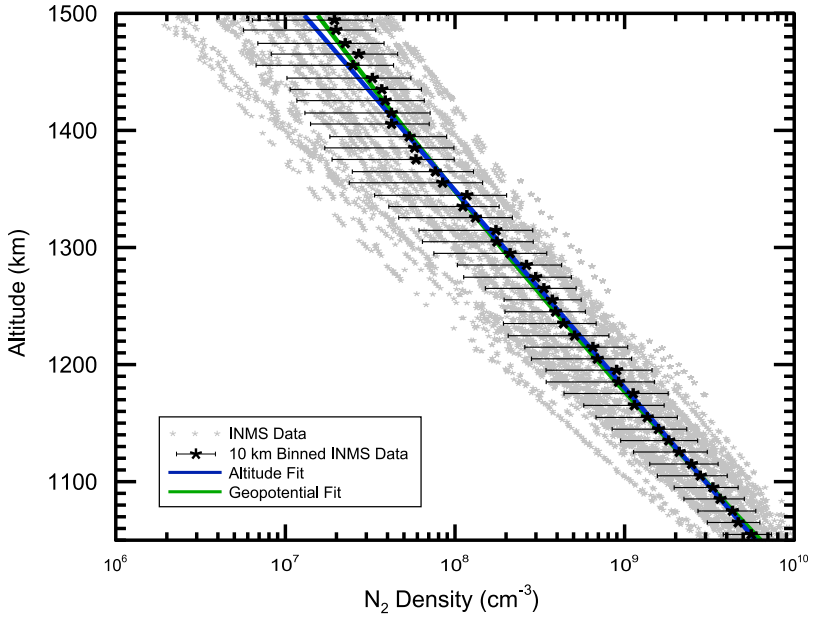

Figure 2. Shown is all of the data presented in this work collected during 29 Titan flybys. The actual data points collected are in gray. The 10 km binned data with the bars representing the standard deviation of the data within the bin are in black. The binned data are not used to produce the fits and are shown solely to illustrate the nitrogen density trend. The blue line gives a linear fit to the logarithm of the density using the altitude, while the green line gives a linear fit using the geopotential height.

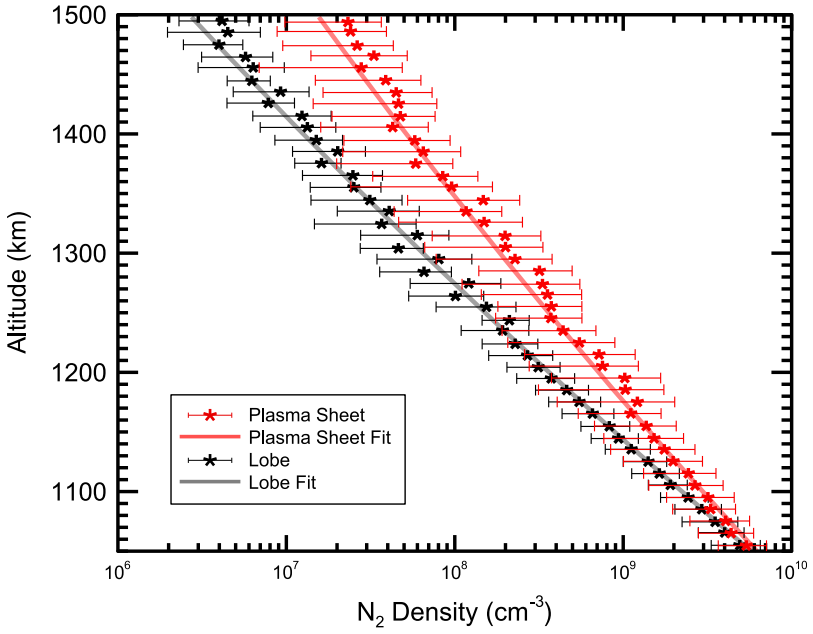

Figure 3. Shown are the binned mass density values for lobe and plasma sheet magnetospheric regions. The flybys identified as plasma sheet are in red, and the lobe-like flybys are in black. The light red line is the fit to the plasma sheet densities, while gray line gives the fit to the lobe densities. The difference in the altitude profiles is, in general, outside of the standard deviation of the mean densities.

indicative of the large magnitude of the heating and was the largest deviation observed between data groupings used in this work. Furthermore, the density decrease results in a roughly 135 km reduction in the exobase height. The bimodal and magnetosheath bins constitute two flybys each and thus have insufficient geospatial and solar coverage to draw any conclusions from. However, it does appear that these plasma environments are in between the heating provided by the plasma sheet and the decreased heating of the lobe type flybys.

[19] Figure 4 shows the temperatures derived on a flyby by flyby basis. The mean effective temperature of the flybys is 140.4 K, a result significantly lower than that obtained by fitting the entirety of the data in a single profile. The difference is likely due to the nonlinearity of the temperature extraction process; the inferred temperature of the mean data set is not equivalent to the mean of the inferred temperatures from each flyby. The presence or absence of the plasma sheet defines the outliers of the temperatures with plasma sheet flybys being the highest in temperature and lobe flybys being the lowest. The mean effective temperature of the plasma sheet flybys is 143.8 K while that of the lobe flybys is 118.2 K, a 25.6 K difference. No solar or geophysical trend is apparent in the observed temperatures.

[20] Two flyby groupings show significant changes in effective temperatures on timescales of 1 Titan day (about 16 Earth days). The T25/T26 and the T55/T56/T57 grouping are nearly identical in flyby trajectory, solar condition, and local plasma configuration and differ only in the identified plasma regime. T25 was identified to be mixed plasma sheet and lobe conditions while T26 was bimodal. The effective temperatures were 171.9 ± 1.7 K and 142.9 ± 1.3 K for the T25 and T26 flybys, respectively. *Simon et al.* [2010] classify the time before the T26 flyby to be within the southern lobe while the entirety of the T25 flyby was within the plasma sheet. The T55/T56/T57 flyby grouping is nearly identical in trajectory with a slight deviation in latitude ranging from 21°S to 42°S. Again, the solar conditions were nearly identical and only the plasma regime differs. The obtained

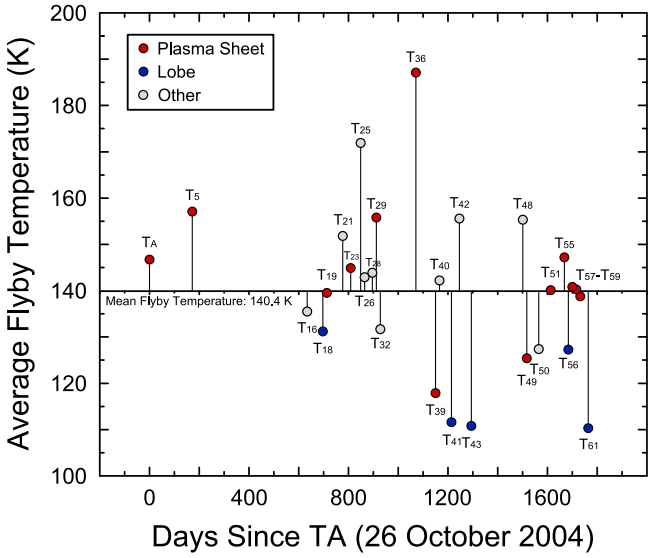

Figure 4. Shown are the single flyby effective temperatures plotted versus time since TA. The red circles represent the plasma sheet flybys, the blue circles show the lobe flybys, and the gray circles give all other classifications. The flyby groupings T25/T26 and T55/T56/T57, which are separated by 1 Titan day (16 Earth days), show that Titan's thermosphere responds to varying plasma environments on timescales less than 1 Titan day.

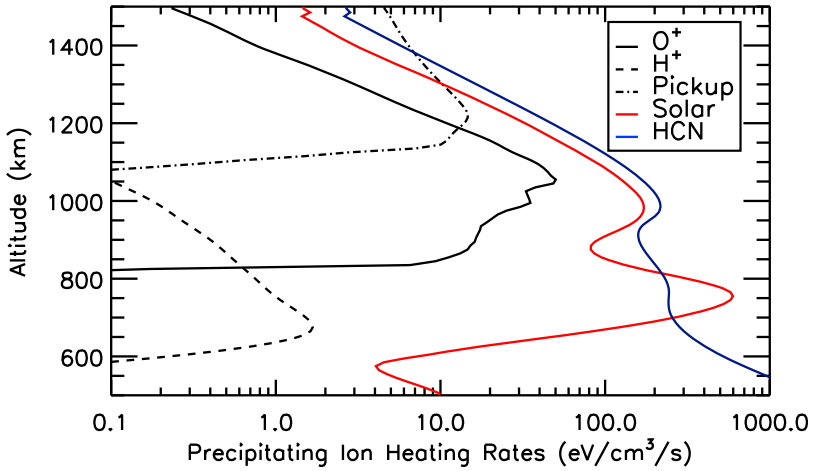

Figure 5. Shown are the heating rates used in the T−GITM model. Altitude profiles of the O^+, H^+, and pickup ion precipitation heating rates are shown. The heating rates for O^+ and H^+ are obtained from *Shah et al.* [2009] and *Smith et al.* [2009], respectively. The pickup ion heating rates are from *Michael and Johnson* [2005]. Also shown is the HCN cooling rate and solar EUV/UV heating rate for comparison.

effective temperatures were 147.2 ± 6.4 K, 127.3 ± 2.5 K, and 140.8 ± 1.5 K for T55, T56, and T57, respectively. T55 and T57 were classified as plasma sheet while T56 is a lobe flyby. These two groupings are separated by 1 Titan day. The T36, T39, and T49 flybys present outliers in the plasma sheet data. The T39/T40 and T48/T49 flybys, though only 1 Titan day apart have very different flyby trajectories and are therefore not expected to isolate the plasma influence. The magnitude of the temperature differences observed between these flybys further indicates that Titan's thermosphere reacts globally on a timescale which is less than 1 Titan day, however some portion of the observed difference may be due to nonplasma related effects.

3.2. Model Results

[21] Next, we employ the Titan Global Ionosphere Thermosphere Model (T-GITM) [*Bell et al.*, 2010a] in order to test whether or not plasma heating can lead to the variations found in the INMS data. We emphasize that we are not attempting to reproduce the exact N_2 density variations identified by the data analysis of the previous sections, but instead we are merely using T-GITM to test whether or not the temperature variations from the data can be reproduced by the model in a gross sense. In order to accomplish this, we employ the one-dimensional (1-D) version of the three-dimensional (3-D) T-GITM framework, which calculates the coupled energetics, dynamics, and composition of Titan's upper atmosphere. In the work given by *Bell et al.* [2010a, 2010b, 2010c], the 1-D model was validated by self-consistently reproducing the average INMS major neutral densities and mixing ratios between TA and T40. T-GITM itself is a nonhydrostatic 3-D Navier-Stokes Global model for the Ionosphere-Thermosphere region of Titan's atmosphere, based upon the Earth Global Ionosphere-Thermosphere Model (GITM) of *Ridley et al.* [2006].

[22] The T-GITM consists of 15 neutral species and 5 ion species that interact chemically through a reduced ion-neutral chemical scheme focused on the production of HCN, C_2H_4, $HCNH^+$, and $C_2H_5^+$. Moreover, the T-GITM includes a self-consistent calculation for the thermal structure using solar EUV/UV forcing, HCN rotational cooling, thermal conduction, and plasma heating. We assume, for the purposes of this study, that we can approximate the plasma influence on Titan's upper atmosphere through the precipitation of O^+ and H^+ ions from Saturn's magnetosphere as well as pickup ions. We adopt the vertical heating profiles from *Shah et al.* [2009] for O^+, from *Smith et al.* [2009] for H^+, and from *Michael and Johnson* [2005] for pickup ions. The vertical heating rates from all species are shown alongside that of the solar EUV/UV photons and the HCN rotational cooling in Figure 5. Above 1200 km, the heating rates for the plasma processes are of the same magnitude as the solar EUV/UV heating. We know that the plasma heating by precipitating ions is located mostly on the corotational ram-side of Titan while the pickup ions deposit their energy primarily on the Saturn-facing side of Titan [*Tseng et al.*, 2008; *Sillanpä et al.*, 2007]. For the moment, we ignore this spatial dependence and utilize a global mean heating rate, scaled so that the column integrated orbit-averaged energy deposition is roughly 6×10^8 eV cm^{-2} s^{-1}. Furthermore, the impact of magnetospheric electrons is neglected as the field configurations around Titan in which the electron precipitation is highly dependent are very complex and are likely significantly different for each pass [*Bertucci et al.*, 2008]. It is also possible that other effects are contributing to the plasma heating such as Joule heating will be treated in subsequent work. The results here are suggestive of the net effect of the thermal response of the thermosphere to a plasma-induced heating process of the magnitude assumed for ion precipitation.

[23] We use two models for Titan's upper atmosphere, one model with plasma heating and one model without plasma heating, as shown in Figures 6 and 7. For each model, the most salient settings and boundary conditions are as follows: (1) $F_{10.7-cm} = 80.0 \times 10^{-22}$ W m^{-2} Hz^{-1}, (2) latitude = 0.0°N (equator), (3) subsolar latitude = ~5.0°S, (4) T_0 = 165.0 K, and (5) $N_0 = 8.7 \times 10^{19}$ molecules m^{-3}.

[24] In the above list, we note that Latitude stands for the latitude of the 1-D model, subsolar latitude is that latitude directly below the Sun, T_0 is the temperature adopted at the model lower boundary at 500 km, and N_0 is the total density

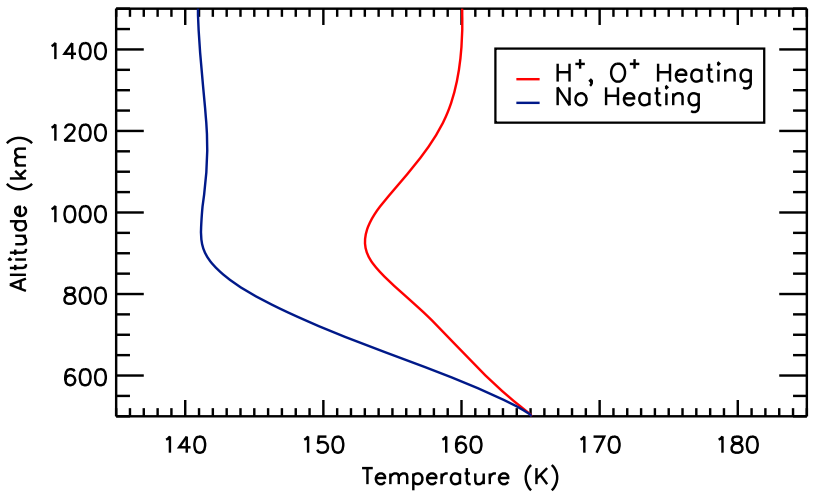

Figure 6. Shown are the temperature profiles retrieved from the two runs of the T-GITM model. The red line gives the simulation with the plasma heating, while the blue line shows the simulation without plasma heating. The temperature deviation is roughly 19 K at the exobase resulting from the plasma heating.

adopted at 500 km. Thus, the only difference between the two models is that one includes plasma heating and one does not; all other parameters are held constant.

[25] Figure 6 contains the resulting diurnally averaged temperature structures from T-GITM. From Figure 6, we note that the plasma heating has a profound impact on the overall thermal structure of the upper atmosphere, as was found previously by *Bell et al.* [2010a]. Exospheric temperatures range from 160 K (heating included) to 141 K (without heating), producing a temperature deviation on the order of 19.0 K between the two models. This is similar the thermal structure deviations of 29.0 K identified between the plasma sheet and lobe flybys.

[26] The diurnally averaged total densities in the upper atmosphere from both models are presented in Figure 7, which shows the wide dichotomy in neutral densities produced by the thermal structures of Figure 6. Upon inspection, one notes that the model that includes plasma heating is consistent with the INMS mass densities during plasma sheet conditions. Similarly, when we exclude plasma heating from T-GITM, we generate the blue curve in Figure 7, which is similar to the INMS densities that occur during the lobe conditions. The heating versus nonheating model results produce a similar dichotomy in effective temperatures and density structures as the plasma sheet versus lobe observations.

4. Discussion

4.1. Comparison With Previous Results

[27] Several methods have previously been utilized to determine the effective or inferred temperature of the upper atmosphere from the INMS measurements. The first and most sophisticated method utilizes a diffusion model with the scale

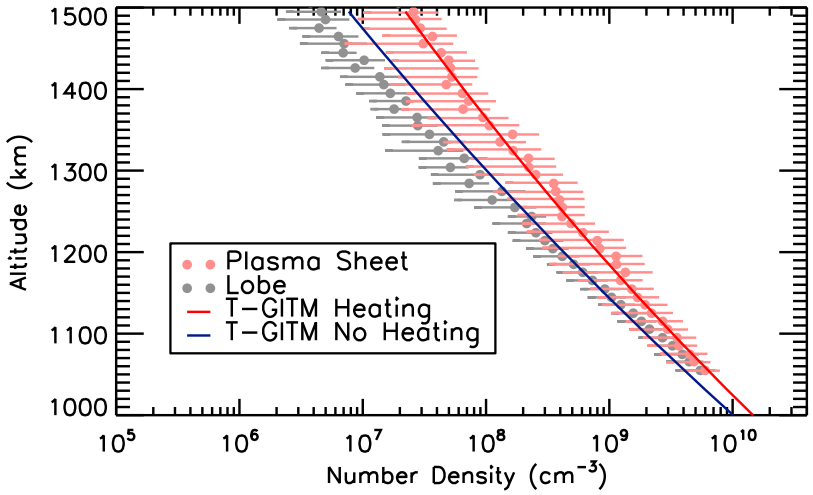

Figure 7. Shown are the density profiles from the T-GITM runs overlaid upon the plasma sheet and lobe densities. The light red circles give the 10 km binned densities from the plasma sheet flybys, while the gray circles give the same for the lobe flybys. The red line gives the resulting nitrogen densities from the T-GITM simulation with plasma heating, while the blue line gives the result without plasma heating.

Table 3. Presented are the Effective Temperatures for the Groupings Listed[a]

	T_{Eff} (K)	*Cui et al.* [2009]
Global average	153.0 ± 0.6	151.0 ± 1.5
Dayside (0600–1800 UT)	148.9 ± 0.8	142.1 ± 1.4
Nightside (1800–0600 UT)	157.0 ± 0.8	154.8 ± 1.5
Northern Hemisphere	152.8 ± 0.8	
Southern Hemisphere	144.4 ± 0.9	
High northern latitude (60N–90N)	142.3 ± 1.4	146.4 ± 1.5
Middle northern latitude (30N–60N)	147.5 ± 1.2	151.2 ± 1.5
Low northern latitude (0–30N)	160.9 ± 1.6	153.4 ± 1.4
Low southern latitude (0–30S)	141.5 ± 1.2	
Middle southern latitude (30S–60S)	163.6 ± 1.5	
Low SZA (0–60)	153.9 ± 1.1	
Mid SZA (60–120)	145.8 ± 1.0	
High SZA (120–180	158.2 ± 1.0	

[a]The fits are taken over the altitude range 1050 km to the calculated exobase height. Also shown for comparison are the values from *Cui et al.* [2009].

height, boundary densities, eddy coefficient, and vertical flux as free parameters [*Waite et al.*, 2005, 2007; *De La Haye et al.*, 2007a; *Yelle et al.*, 2006]. Several assumptions are required when employing this method, including the assumption of either high escape rates or eddy coefficients to fit the spectrum, yielding multiple solutions that are not unique. It should be noted however that the tradeoff between eddy coefficients and escape rates primarily impacts the interpretation of the observed methane mixing ratios and plays a minor role in determining the thermal structures. Top down pressure integration yields temperature profiles below the exobase. This method is susceptible to both the choice of pressure, and hence temperature, at the top of the atmosphere and to horizontal movements in the spacecraft [*Müller-Wodarg et al.*, 2008]. Finally, it is possible to determine the scale height directly from the slope of the measured densities utilizing the hydrostatic equation as performed in this study. This method is not dependent on boundary conditions and relies solely on the assumption that the atmosphere is hydrostatic and isothermal in the upper thermosphere; an assumption which has been shown to be in good agreement locally with the measured N_2 densities [*Waite et al.*, 2005]. This method has been used considering the flybys T5-T37 [*Cui et al.*, 2009] and to obtain preliminary results for the spatial variation in coronal heating [*Johnson et al.*, 2009].

[28] Shown in Table 3 are the fit results for an array of solar and dynamical parameters. The effective temperature was obtained from the mean scale height as fit to the collection of data points which lie in the specified bin in the altitude range between 1050 km and the exobase. Titan's dayside is observed to have an effective temperature of 148.9 ± 0.8 while the night side has an effective temperature of 157.0 ± 0.8. The observation of an 8.1 K greater effective temperature on Titan's nightside is suggestive of significant nonsolar heating sources (i.e., magnetospheric heating and/or global dynamics). A greater fraction of the nightside flybys sampled occur during plasma sheet interactions which are likely the cause of the greater nightside temperatures. *Müller-Wodarg et al.* [2008] posit that in the northern hemisphere there appears to be a latitudinal temperature and density dependence. This dependency was then likened to an oblateness in the thermosphere. However, the southern hemisphere presents no regular organization like that of the northern hemisphere. *Müller-Wodarg et al.* [2008] further noted that the observed density structure did not show a systematic trend with solar zenith angle. Our study found that observations during the greatest SZAs yielded the greatest temperatures, a result atypical for a solar driven atmosphere. Furthermore, within the flybys assessed by *Müller-Wodarg et al.* [2008] (T5-T32) the lowest northern latitude passes (T23, T25, and T26) were within the plasma sheet for most of the time leading up to the flyby [*Simon et al.*, 2010]. The highest northern latitude passes (T5, T16, T18, T32) were more mixed but were more frequently within the southern lobe region. The coincidental correlation between the plasma environment and the latitude may have led to the assessment that the densities and thermospheric structure were latitudinally dependent rather than dependent on the plasma environment. Our study however finds no global correlation with latitude or solar zenith angle that would indicate that the upper thermospheric structure is solar driven.

4.2. Implications of Plasma Influence on Titan's Upper Atmosphere

[29] The altitude of maximum energy deposition, as shown in Figure 5, for thermal plasma processes is in general at altitudes above the solar EUV/UV energy deposition. The observation of weak dependence of the upper thermospheric temperature on solar parameters appears to reinforce this. Throughout the flybys covered in this study the Sun was in a particularly quiet solar minimum; the F10.7 cm solar radio flux ranges from 66 to 137 solar flux unit (sfu) with a mean value of 76 sfu which is well within the solar minimum range, and significantly below the robust F10.7 cm value of 183 sfu observed during the Voyager encounter. The solar forcing may therefore be substantially subdued due to its apparent inactivity during the time span of the measurements. Therefore, since solar heating is not expected to dominate in the region investigated and the solar forcing is at its relative minimum the external heating from solar EUV/UV photons would be expected to have a diminished effect on the upper atmospheric density and temperature profiles.

[30] Complex chemical feedback systems within the thermosphere are likely to contribute to the heat budget of Titan. HCN is linked to the thermal balance through not only diffusion processes but also through photochemical processes. Electron recombination of the primary ionospheric ion, $HCNH^+$ whose abundance is largely solar controlled [*Agren et al.*, 2009], is the major production pathway for HCN. The cooling ability of HCN is unmatched in Titan's thermosphere and is the major controller of the thermal structure [*Yelle*, 1991]. The production of HCN seems to effectively mitigate the solar heating through a chemical feedback system. This proceeds in the following fashion: increased solar EUV/UV produces enhanced $HCNH^+$, which then increases the abundance of HCN, finally HCN radiates away the heat. This process will reduce the local effect of the solar heating while atmospheric convection will quickly distribute any localized heating source throughout the atmosphere. The impact of oxygen ion deposition is not expected to drastically influence the chemistry of the upper atmosphere [*Hörst et al.*, 2008]; therefore chemical regulation feedbacks may be less important for this particular heating process. Pickup ions are expected to chemically react in the upper atmosphere, possibly leading to a thermal feedback. The

absence of feedbacks leading to cooling may result in the observed thermal structures. Further studies of the effect of minor species on solar or plasma heating are needed.

[31] It is observed that Titan's thermosphere reacts to the plasma environment on a timescale of the order or less than 1 Titan day (16 Earth days). This is evident from the large deviations between the T25/T26 and T55/T56/T57 flyby groupings. The northern hemisphere T25/T26 show a 29.0 K effective temperature difference. The trajectory and solar conditions were nearly identical for these two flybys, although the plasma was observed to deviate. *Müller-Wodarg et al.* [2008] note that the T25 and T26 flybys differ in density structure by roughly a factor of 2. *Rymer et al.* [2009] state that T25 is a mixed flyby with plasma sheet and lobe portions while T26 is bimodal; *Simon et al.* [2010] show that the ingress of T26 occurs within the southern lobe which is expected to be the region of least plasma influence. The T55/T56/T57 flyby grouping contains three flybys which are identical in nearly every respect and take place 1 Titan day apart. Effective temperatures of 147.2 ± 3.2 K, 127.3 ± 2.5 K, and 140.8 ± 1.5 K are observed for T55, T56, and T57, respectively. T55 and T57 were identified as a plasma sheet flybys while T56 is a lobe flyby. The temperature differences between these flybys are likely indicative of the plasma heating occurring when Titan is influenced by the plasma sheet. These flyby groupings suggest the relatively fast response of the thermosphere to the change in plasma conditions.

[32] Other processes linked to the plasma environment such as Joule heating and pickup ion deposition will likely contribute to the thermospheric heating. It is likely that Titan will experience substantial amounts of Joule heating due to the variable plasma and magnetic environment in addition to the observed ion precipitation. The extent of the effect of Joule heating on the thermosphere is currently unknown.

5. Conclusions

[33] Titan's thermospheric structure can, in principle, be influenced by Saturn's magnetospheric plasma [*Johnson*, 2009]. Dense, energetic plasmas observed within the plasma sheet have been shown to heat the thermosphere possibly through O^+ and H^+ ion precipitation. Such processes could account for effective temperatures found here to be on average 29.0 K greater than those observed in the sparse, cold lobe plasmas. The propensity of Saturn's magnetospheric plasma to deposit heat into Titan's thermosphere is most clearly shown when assessing INMS data with respect to the plasma environment during the flyby. The plasma influence on Titan's upper atmosphere first suggested by the analysis of the earlier results from the INMS instrument [*De La Haye et al.*, 2007a] is now evident in the large effective temperature difference observed between the dense, energetic plasma sheet encounters and the sparse lobe encounters. The magnitude of the temperature deviation is significantly greater than those obtained by grouping the flybys by solar parameters. Navier-Stokes modeling utilizing the T-GITM model further illustrated that the observed density differences can be replicated with appropriate plasma parameters based on CAPS observations. The plasma influence has therefore likely been the driver of the upper atmospheric thermal structure throughout the Cassini mission to date.

[34] The thermosphere was observed to respond to plasma heating on a timescale of 1 Titan day (16 Earth days) or less. Flybys with nearly identical trajectories and solar conditions but different plasma conditions are observed to have large effective temperature differences. Fortuitously these flybys occurred within 1 Titan day. This observation leads to the conclusion that Titan's thermosphere responds to the plasma environment on a timescale less than the time between these flybys. Further investigations using time dependent, coupled models are necessary to further investigate this effect.

[35] The thermospheric temperatures show little or no correlation with solar parameters. This is possibly due to reduced solar activity and fluxes during the extended solar minimum in which the observations took place, or indicative of the effectiveness of the photochemical feedback mechanism in Titan's upper atmosphere in regulating the heat provided by solar photons. The Cassini solstice mission extending observations of Titan until 2017 will allow for observations of the thermosphere during solar maximum conditions.

Appendix A: Assessment of Systematic Uncertainties

[36] *Müller-Wodarg et al.* [2008] noted that the trajectory of the Cassini spacecraft through Titan's upper atmosphere could yield significant horizontal deviations within a vertical density profile. This is due to the large swaths of area transversed by the Cassini spacecraft when near closest approach. If significant horizontal structure exists in Titan's upper atmosphere this would affect the temperature structure obtained through the assumption of purely vertical motions. To ascertain the extent to which systematic density perturbations such as meridional and zonal bulges affect the effective temperature derivation a simplistic model of Titan's upper atmosphere was constructed. The atmospheric mass density was defined as dependent on geopotential altitude by the following:

$$\rho = \rho_0 \exp\left(\frac{z - z_0}{H_0}\right) * (1 + f(\phi, \lambda)), \tag{A1}$$

where z_0 is the reference altitude and H_0 is the reference scale height, in this case defined as 1000 km with the scale height fixed using an effective temperature of 148 K. The density was then perturbed through the function $f(\phi, \lambda)$, creating a confined density variation. Physically the density perturbations correspond to atmospheric changes outside of the observation altitude which modify the isobaric surface. Two models were chosen, one which represented a latitudinal bulge of twice the nominal density at the equator than the pole (Model 1) and another representing a convolution of two density bulges, one in longitude and one in latitude (Model 2). The choice of models is motivated by previous works by *Müller-Wodarg et al.* [2008] in which it is shown that the INMS data may present systematic density perturbations aligned with geospatial parameters. Model 1 is motivated by the latitudinal bulge reported in the INMS data by *Müller-Wodarg et al.* [2008]; Model 2 represents potentially aligned forcings from solar and plasma effects. The magnitude of the perturbations were chosen to match those previously published.

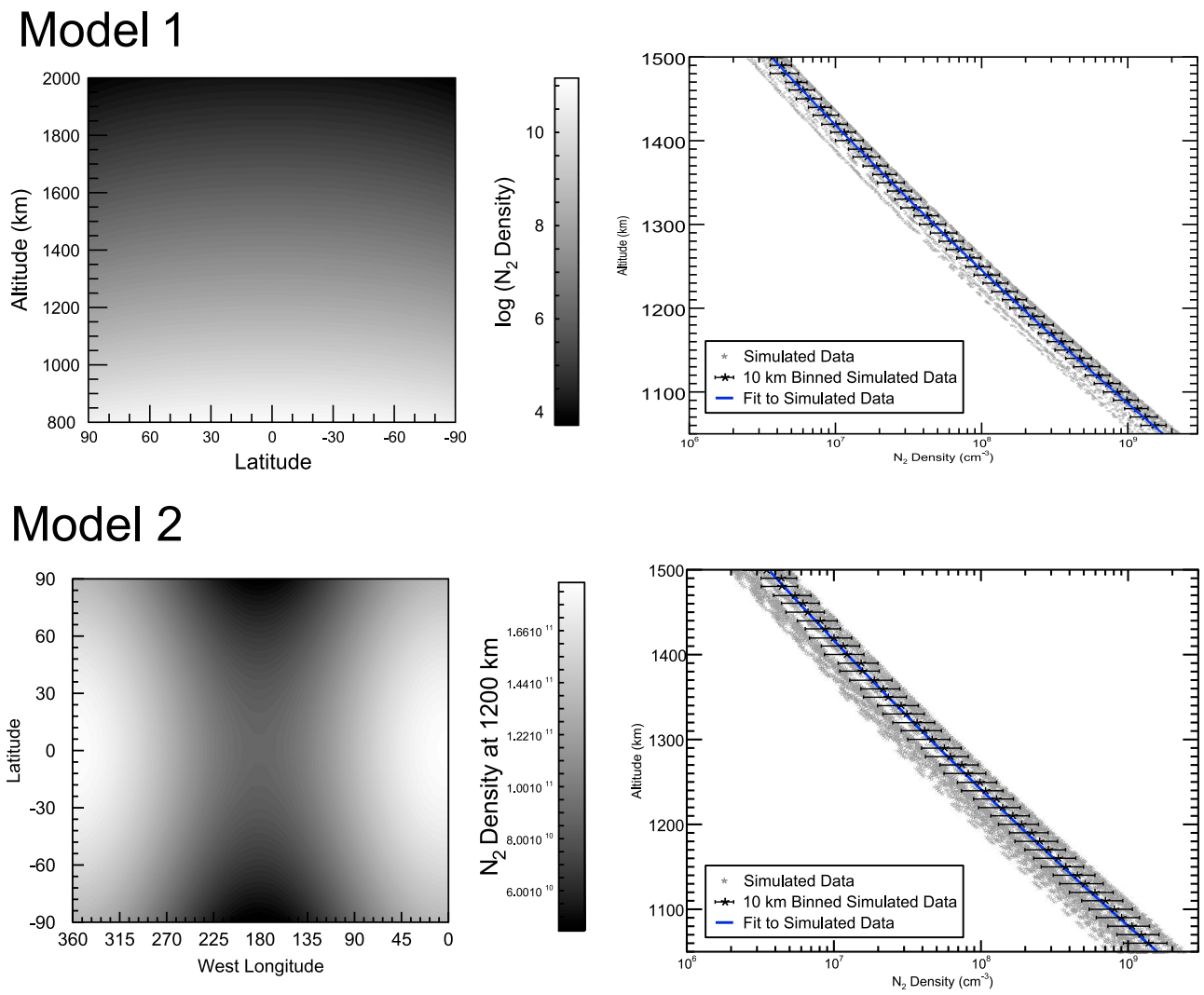

Figure A1. Shown are the model densities and resulting altitude profiles for the two test cases explored. (top) Model 1 consists of a purely latitudinally cosine function dependent density structure with a factor of 2 difference from the pole to the equator. (bottom) Model 2 changes by both the cosine of the latitude and longitude. The right-hand plots show the resulting densities and global fits.

[37] Once the three-dimensional density structure was produced the Cassini INMS targeted flybys were then flown through the model atmosphere. The resulting densities were binned and effective temperatures determined using the same method as presented in section 2. To verify the functionality of the model a flat atmosphere ($f(\phi, \lambda) = 0$) was produced and verified to obtain the 148.0 K temperature.

[38] Model 1, shown in Figure A1 (top) produces a range of temperatures from 147.2 K to 149.4 K with a mean temperature of 148.4 K. The resulting total temperature deviation of 2.2 K is close enough to the average effective temperature uncertainty to be neglected. Model 2, whose results are shown in Figure A1 (bottom) exhibits a range of binned effective temperatures from 145.1 K to 153.1 K a total difference of 8 K. This effect could possibly mask lower-order heating processes in the upper atmosphere, especially those which result in temperature deviations of less than 10 K. However, it is clear that this effect cannot reasonably account for the magnitude of the deviations observed between the plasma sheet and the lobe flybys.

[39] *De La Haye et al.* [2007a] noted that a significant population of suprathermal N_2 existed near the exobase on some flybys. This population is manifest in the drastic upturn in the density profiles above the exobase and in general results in a 10–20 K temperature increase. *De La Haye et al.* [2007b] calculated the density of suprathermal N_2 to be roughly 5 orders of magnitude less in density than the thermal population and decreases significantly as the atmospheric

Table A1. Shown are the Effective Temperatures Obtained by Various Mean Scale Height Fits on the TA Flyby[a]

Boundary Altitude (km)	T_{Eff} (K)
1597.5 (exobase height)	146.7 ± 1.6
1650.0	146.7 ± 1.5
1700.0	146.9 ± 1.5
1750.0	147.4 ± 1.4
1800.0	147.9 ± 1.3

[a]The fits varied the upper boundary altitude to either neglect or incorporate exospheric populations.

density increases. We assessed the potential effects of a suprathermal population on the obtained effective temperatures by selecting the TA flyby which *De La Haye et al.* [2007a] stated had a significant suprathermal population at the exobase and performing the mean scale height fits at various altitudes both above and below the exobase. The results of this study are shown in Table A1. The difference in obtained effective temperatures is at most 1.2 K, or 0.8%. This result shows that when averaged over the upper thermosphere the effective temperature is not affected by the suprathermal populations at the exobase.

[40] **Acknowledgments.** This work was supported by NASA Headquarters under the NASA Earth and Space Science Fellowship Program grant NNX08AW24H.

[41] Masaki Fujimoto thanks the reviewers for their assistance in evaluating this paper.

References

Agren, K., J.-E. Wahlund, P. Garnier, R. Modolo, J. Cui, M. Galand, and I. Mueller-Wodarg (2009), On the ionospheric structure of Titan, *Planet. Space Sci.*, *57*, 1821–1827.

Arridge, C. S., K. K. Khurana, C. T. Russell, D. J. Southwood, N. Achilleos, M. K. Dougherty, A. J. Coates, and H. K. Leinweber (2008), Warping of Saturn's magnetospheric and magnetotail current sheets, *J. Geophys. Res.*, *113*, A08217, doi:10.1029/2007JA012963.

Banks, P. M., and G. Kockarts (1973), *Aeronomy*, Academic, New York.

Bell, J. M., et al. (2010a), Simulating the one-dimensional structure of Titan's upper atmosphere: 1. Formulation of the Titan Global Ionosphere-Thermosphere Model and benchmark simulations, *J. Geophys. Res.*, *115*, E12002, doi:10.1029/2010JE003636.

Bell, J. M., et al. (2010b), Simulating the one-dimensional structure of Titan's upper atmosphere: 2. Alternative scenarios for methane escape, *J. Geophys. Res.*, *115*, E12018, doi:10.1029/2010JE003638.

Bell, J. M., et al. (2010c), Simulating the one-dimensional structure of Titan's upper atmosphere: 3. Mechanisms determining methane escape, *J. Geophys. Res.*, doi:10.1029/2010JE003639, in press.

Bertucci, C., et al. (2008), The magnetic memory of Titan's ionized atmosphere, *Science*, *321*, 1475–1478.

Chapman, S., and T. G. Cowling (1952), *The Mathematical Theory of Non-Uniform Gases*, Cambridge Univ. Press, Cambridge, U. K.

Coates, A. J. (2010), Interaction of Titan's ionosphere with Saturn's magnetosphere, *Phil. Trans. R. Soc. A*, *367*, 773–788.

Cui, J., et al. (2009), Analysis of Titan's neutral upper atmosphere from Cassini Ion Neutral Mass Spectrometer measurements, *Icarus*, *200*, 581–615.

Cravens, T. E., I. P. Robertson, S. A. Ledvina, D. Mitchell, S. M. Krimigis, and J. H. Waite Jr. (2008), Energetic ion precipitation at Titan, *Geophys. Res. Lett.*, *35*, L03103, doi:10.1029/2007GL032451.

De La Haye, V., et al. (2007a), Cassini Ion and Neutral Mass Spectrometer data in Titan's upper atmosphere and exosphere: Observation of a suprathermal corona, *J. Geophys. Res.*, *112*, A07309, doi:10.1029/2006JA012222.

De La Haye, V., J. H. Waite Jr., T. E. Cravens, A. F. Nagy, R. E. Johnson, S. Lebonnois, and I. P. Robertson (2007b), Titan's corona: The contribution of exothermic chemistry, *Icarus*, *191*, 236–250.

De La Haye, V., J. H. Waite Jr., T. E. Cravens, S. W. Bougher, I. P. Robertson, and J. M. Bell (2008), Heating Titan's upper atmosphere, *J. Geophys. Res.*, *113*, A11314, doi:10.1029/2008JA013078.

Fulchignoni, M., et al. (2005), In situ measurements of the physical characteristics of Titan's environment, *Nature*, *438*, 785–791.

Hartle, R. E., et al. (2006), Initial interpretation of Titan plasma interaction as observed by the Cassini plasma spectrometer: Comparisons with Voyager 1, *Planet. Space Sci.*, *54*, 1211–1224.

Hörst, S. M., V. Vuitton, and R. V. Yelle (2008), Origin of oxygen species in Titan's atmosphere, *J. Geophys. Res.*, *113*, E10006, doi:10.1029/2008JE003135.

Johnson, R. E. (2009), Sputtering and heating of Titan's upper atmosphere, *Phil. Trans. R. Soc.*, *367*, 753–771.

Johnson, R. E., O. J. Tucker, M. Michael, E. C. Sittler, H. T. Smith, D. T. Young, and J. H. Waite (2009), Mass loss processes in Titan's upper atmosphere, in *Titan From Cassini-Huygens*, edited by R. H. Brown, J.-P. Lebreton, and J. H. Waite, pp. 373–391, Springer, Dordrecht, Neth.

Magee, B. A., J. H. Waite, K. E. Mandt, J. H. Westlake, J. Bell, and D. A. Gell (2009), INMS derived composition of Titan's upper atmosphere: Analysis methods and model comparison, *Planet. Space Sci.*, *57*, 1895–1916.

Michael, M., and R. E. Johnson (2005), Energy deposition of pickup ions and heating of Titan's atmosphere, *Planet. Space Sci.*, *53*, 1510–1514.

Müller-Wodarg, I. C. F., R. V. Yelle, J. Cui, and J. H. Waite (2008), Horizontal structures and dynamics of Titan's thermosphere, *J. Geophys. Res.*, *113*, E10005, doi:10.1029/2007JE003033.

Nemeth, Z., K. Szego, G. Erdos, L. Foldy, A. Rymer, M. F. Thomsen, E. C. Sittler, A. J. Coates, and A. Wellbrock (2009), Global features of ion distributions near Titan, *Eos Trans. AGU*, *90*(52), Fall Meet. Suppl., Abstract SM23C-1642.

Ridley, A. J., Y. Deng, and G. Toth (2006), The global ionosphere thermosphere model, *J. Atmos. Sol. Terr. Phys.*, *68*, 839–864.

Rymer, A. M., H. T. Smith, A. Wellbrock, A. J. Coates, and D. T. Young (2009), Discrete classification and electron energy spectra of Titan's varied magnetospheric environment, *Geophys. Res. Lett.*, *36*, L15109, doi:10.1029/2009GL039427.

Shah, M. B., C. J. Latimer, E. C. Montenegro, O. J. Tucker, R. E. Johnson, and H. T. Smith (2009), The implantation and interactions of O+ in Titan's atmosphere: Laboratory measurements of collision-induced dissociation of N_2 and modeling of positive ion formation, *Astrophys. J.*, *703*, 1947–1954.

Shemansky, D. E., A. I. F. Stewart, R. A. West, L. W. Esposito, J. T. Hallett, and X. Liu (2005), The Cassini UVIS stellar probe of the Titan atmosphere, *Science*, *308*, 978–982.

Sillanpää, I., E. Kallio, R. Jarvinen, and P. Janhunen (2007), Oxygen ions at Titan's exobase in a Voyager 1–type interaction from a hybrid simulation, *J. Geophys. Res.*, *112*, A12205, doi:10.1029/2007JA012348.

Simon, S., A. Wennmacher, F. M. Neubauer, C. L. Bertucci, H. Kriegel, J. Saur, C. T. Russell, and M. K. Dougherty (2010), Titan's highly dynamic magnetic environment: A systematic survey of Cassini magnetometer observations from flybys TA-T62, *Planet. Space Sci.*, *58*, 1230–1251.

Sittler, E. C., R. E. Hartle, C. Bertucci, A. Coates, T. Cravens, I. Dandouras, and D. Shemansky (2009), Energy deposition processes in Titan's upper atmosphere and its induced magnetosphere, in *Titan From Cassini-Huygens*, edited by R. H. Brown, J.-P. Lebreton, and J. H. Waite, pp. 393–453, Springer, Dordrecht, Neth.

Smith, H. T., D. G. Mitchell, R. E. Johnson, and C. P. Paranicas (2009), Investigation of energetic proton penetration in Titan's atmosphere using the Cassini INCA instrument, *Planet. Space Sci.*, *57*, 1538–1546.

Strobel, D. F. (2008), Titan's hydrodynamically escaping atmosphere, *Icarus*, *193*, 588–594.

Strobel, D. F. (2009), Titan's hydrodynamically escaping atmosphere: Escape rates and the structure of the exobase region, *Icarus*, *202*, 632–641.

Tseng, W.-L., W.-H. Ip, and A. Kopp (2008), Exospheric heating by pickup ions at Titan, *Adv. Space Res.*, *42*, 54–60.

Vervack, R. J., B. J. Sandel, and D. F. Strobel (2004), New perspectives on Titan's upper atmosphere from a reanalysis of the Voyager 1 UVS solar occultations, *Icarus*, *170*, 91–112.

Waite, J. H., Jr., et al. (2005), Ion neutral mass spectrometer results from the first flyby of Titan, *Science*, *308*, 982–986.

Waite, J. H., Jr., D. T. Young, T. E. Cravens, A. J. Coates, F. J. Crary, B. Magee, and J. Westlake (2007), The process of tholin formation in Titan's upper atmosphere, *Science*, *316*, 870–875.

Yelle, R. V. (1991), Non-LTE models of Titan's upper atmosphere, *Astrophys. J.*, *383*, 380–400.

Yelle, R. V., N. Borggren, V. de la Haye, W. T. Kasprzak, H. B. Niemann, I. C. F. Müller-Wodarg, and J. H. Waite Jr. (2006), The vertical structure of Titan's upper atmosphere from Cassini Ion Neutral Mass Spectrometer measurements, *Icarus*, *182*, 567–576.

J. M. Bell, B. A. Magee, K. E. Mandt, and J. H. Waite Jr., Space Science and Engineering Division, Southwest Research Institute, 6220 Culebra Rd., San Antonio, TX 78228, USA. (jbell@swri.edu)

R. E. Johnson, Engineering Physics Program, University of Virginia, Charlottesville, VA 22904, USA.

J. G. Luhmann, Space Sciences Laboratory, University of California, Berkeley, CA 94720, USA.

A. M. Rymer, Johns Hopkins University Applied Physics Laboratory, Laurel, MD 20723, USA.

J. H. Westlake, Department of Physics and Astronomy, University of Texas at San Antonio, One UTSA Blvd., San Antonio, TX 78249, USA. (jwestlake@swri.edu)